

Electrochemical Fine-Tuning of the Chemoresponsiveness of Langmuir–Blodgett Graphene Oxide Films

Juan M. Devida, Facundo Herrera, M. Antonieta Daza Millone, Félix G. Requejo,* and Diego Pallarola*

Cite This: *ACS Omega* 2023, 8, 27566–27575

Read Online

ACCESS |



Metrics & More

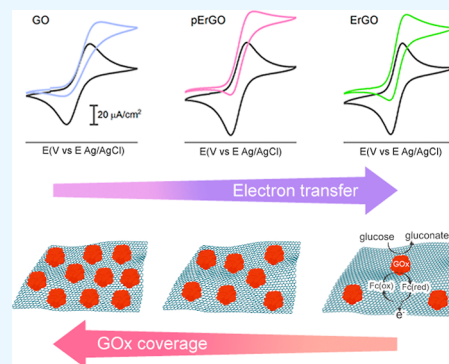


Article Recommendations



Supporting Information

ABSTRACT: Graphene oxide has been widely deployed in electrical sensors for monitoring physical, chemical, and biological processes. The presence of abundant oxygen functional groups makes it an ideal substrate for integrating biological functional units to assemblies. However, the introduction of this type of defects on the surface of graphene has a deleterious effect on its electrical properties. Therefore, adjusting the surface chemistry of graphene oxide is of utmost relevance for addressing the immobilization of biomolecules, while preserving its electrochemical integrity. Herein, we describe the direct immobilization of glucose oxidase onto graphene oxide-based electrodes prepared by Langmuir–Blodgett assembly. Electrochemical reduction of graphene oxide allowed to control its surface chemistry and, by this, regulate the nature and density of binding sites for the enzyme and the overall responsiveness of the Langmuir–Blodgett biofilm. X-ray photoelectron spectroscopy, surface plasmon resonance, and electrochemical measurements were used to characterize the compositional and functional features of these biointerfaces. Covalent binding between amine groups on glucose oxidase and epoxy and carbonyl groups on the surface of graphene oxide was successfully used to build up stable and active enzymatic assemblies. This approach constitutes a simple, quick, and efficient route to locally address functional proteins at interfaces without the need for additives or complex modifiers to direct the adsorption process.



INTRODUCTION

The use of graphene and its derivatives as nanosupports for a variety of electrochemical biointerfaces has experienced a sustainable growth in the past few years.^{1,2} This can be attributed to their many functional properties that can be exploited to facilitate electrical transduction between biomolecules and the electrode surface. The one-atom-thick planar sheet of carbon atoms densely packed in a honeycomb crystal lattice has remarkable electronic and electrochemical properties that are superior to those found in other nanostructured carbon materials.^{3–6}

Among graphene derivatives, graphene oxide (GO), and its general reduced form (rGO) are extensively used for biosensing applications.⁷ GO is a highly oxidized form of chemically modified graphene, which contains various oxygen functional groups including hydroxyl, epoxy, carbonyl, and carboxyl groups on the basal plane as well as along the edges.⁸ The presence of these functional groups facilitates the surface functionalization of GO, which is of utmost importance for developing biosensors.⁹ rGO is usually obtained by the reduction of GO sheets by chemical, biological, electrochemical, thermal, and photo-mediated methods.¹⁰ These procedures, additionally to the reduction of oxygen, introduce defects in the carbon network that leads to high electrochemical activity compared with that of GO.^{11–13} Therefore, tuning the surface chemistry of graphene-based sheets is key to achieve effective immobilization of biomolecules, while

maintaining high electrical conductivity. Direct electrochemical reduction of GO is arguably the best approach to fabricate rGO-based thin films.^{10,14,15} This method is advantageous over the methods mentioned above regarding that is easy to control the reduction process, it can be performed in mild reaction conditions and it requires no dangerous or environmentally hazardous chemicals.^{10,16,17}

The fabrication of graphene films on various substrates have been realized via several well-established methods, including spin- or spray-coating,¹⁸ drop-casting,¹⁹ dip-coating,²⁰ transfer printing,²¹ electrophoretic deposition,²² and Langmuir–Blodgett (LB) assembly.²³ Among these methods, since it is possible to interact with the film by the barriers fixing border conditions, differently from auto-assembled systems, LB assembly is an appropriate approach capable for controlling the thickness and uniformity of graphene-coated films, which influence the optical and electrical properties of the resultant assembly.²⁴

Received: May 9, 2023

Accepted: July 10, 2023

Published: July 21, 2023



In the present work, we have tuned the density of oxygen-containing functional groups on LB GO films in order to provide chemical functionalization while preserving their electrochemical responsiveness. GO LB films were assembled onto ITO-coated glass and then subjected to electrochemical reduction to achieve GO with different degrees of oxidation. The introduction of glucose oxidase (GOx), through one-step chemical bonding to the surface of GO, yielded a chemoresponsive bioelectrochemical interface. The amount of immobilized GOx was determined by surface plasmon resonance (SPR) spectroscopy. Knowing the enzyme coverage allowed us to evaluate the performance of the enzymatic assembly by measuring the electrochemical response of GOx to glucose. The resulting bioelectrodes could well retain the enzymatic activity of GOx and exhibited efficient electron transfer being able to convert glucose into an electrical signal.

MATERIALS AND METHODS

Reagents and Materials. Glucose oxidase (GOx) from *Aspergillus niger* was purchased from Sorachim SA, Switzerland. ITO substrates (35 Ω /sq) were purchased from Thin Film Devices, USA. Au-coated glass SPR substrates were acquired from BioNavis Ltd., Finland. Ferrocenemethanol and aminoferrocene was acquired from Merck, Argentina. All other reagents were analytical grade.

GO Synthesis, Purification, and Dispersion Preparation. GO was synthesized from graphite flakes using an improved version of the method developed by Marcano et al.²⁵ Briefly, KMnO₄ (6 wt equiv) was slowly added under stirring to a 9:1 mixture of concentrated H₂SO₄/H₃PO₄. Graphite flakes (1 wt equiv) were then added to form a uniform suspension. The reaction was heated to 50 °C and left stirring for 12 h. Then, it was cooled at room temperature and poured onto ice water (200 mL) containing H₂O₂ (30%, 1.5 mL). A change in color of the solution from dark brown to w was observed. The decanted solid was washed with a solution of 30% HCl and then centrifuged at 6500 rpm for 30 min. The resulting precipitate was then dispersed in deionized (DI) water. This procedure was repeated several times (three to five times) until all visible particles were removed from the precipitate. Purity was checked by measuring the conductivity of the supernatant (less than 90 M Ω cm). GO dispersions at 4 mg/mL were made by collecting precipitates and mixing them with water.

Langmuir–Blodgett Assembly of GO Thin Films. GO aqueous solutions were prepared using a method based on a protocol previously reported by Cote et al.²³ The stock dispersion and a 5:1 water/methanol solution were mixed to obtain a 0.15 mg/mL solution. The mixture was sonicated for 30 min and centrifuged twice to obtain a homogeneous GO flakes size distribution. First, the solution was centrifuged at 6500 rpm for 30 min to remove small GO flakes and byproducts from the supernatant. Then, the precipitate was collected and redispersed in a 5:1 water/methanol solution. The resulting suspension was then centrifuged at 2500 rpm for 10 min to remove large GO flakes and aggregates. We used the resulting supernatant in the LB assembly procedure.

For LB assembly, the trough (KSV NIMA, model 5000), placed on an anti-vibration table, was cleaned with chloroform and filled with water. A tensiometer attached to a Pt Wilhelmy plate was used for monitoring surface pressure during compression by moving the two opposing barriers toward each other. Water-air interface impurities were eliminated until

surface pressure was lower than 0.2 mN/m. 5.5 mL of GO suspension were slowly spread on the interface by dropwise addition using a glass syringe. The monolayer-like film formed was stabilized for about 15 min before compression. At the end of the compression, a GO monolayer-like film with a faint brown color could be observed. The GO film was transferred at 15 mN/m to an ITO-coated glass substrate by vertically dipping into the trough and slowly pulling it up at a speed of 0.1 mm/min. The transferred substrates were heated at 80 °C for 1 h to rapidly evaporate water between GO sheets and ITO.

Prior to use, ITO substrates were cleaned with acetone at 50 °C for 20 min in an ultrasound bath and subsequently the procedure was repeated with isopropanol. Then, ITO substrates were rinsed with water and treated with 1:1:5 NH₄OH 27%/H₂O₂ 20%/H₂O solution for 15 min at 70 °C. Finally, ITO substrates were rinsed with water and store under water until use.

For SPR assays, Au-coated glass substrates (BioNavis Ltd.) were used. GO assembly was performed using the same protocol described for ITO-coated glass substrates.

Electrochemical Reduction of GO. Fabrication of partially electrochemically reduced GO (pErGO) and fully electrochemically reduced (ErGO) was carried out through a two-step procedure. First, a thin film of GO was deposited by LB method onto an ITO-coated glass. Then, the electrochemical reduction was carried out using a three-electrode configuration with GO assembly as working electrode, an Ag/AgCl (3 M KCl) as reference electrode and a platinum mesh as counter electrode. The electrochemical reduction was performed with an Autolab PGSTAT302N potentiostat (Metrohm) in PBS pH 7.4 by cycling the potential from 0.0 to -1.1 V at a scan rate of 50 mV/s.

X-ray Photoelectron Spectroscopy Characterization of GO-Based Films. X-ray photoelectron spectra were obtained using a multi-technical surface equipment SPECS with a monochromatic Al K α X-ray source operated at 300 W. A PHOBIOS 150 hemispheric analyzer was used to obtain C 1s signal. The GO, pErGO, and ErGO samples were mounted onto a copper tape and placed under UHV for 12 h before the measurements. The pressure during the measurements was kept below 20⁻⁹ mbar. Quantitative analysis was performed with CasaXPS software by assigning the peaks for each characteristic functional group according to literature.^{26–28} The intensities were estimated by calculating the integral of each peak after subtraction of the S-shaped background and fitting the experimental peak to a Lorentzian/Gaussian mix of variable proportion. In order to quantify atomic percentages for each sample, all spectra were normalized using the Si 2p peak contribution from ITO glass as reference. At least three independent samples were analyzed at each condition.

SPR Spectroscopy. Multiparametric SPR (MP-SPR) experiments were carried out with a SPR-Navi 210A instrument (BioNavis Ltd.). All experiments were performed at a flow rate of 10 μ L/min in PBS pH 7.4 at 22 °C. GOx was used at a concentration of 10 μ M in PBS buffer. To estimate the GOx surface coverage, the SPR angle of minimum reflectivity, θ_{\min} , was measured in situ during the adsorption process. Then, the angle of minimum reflectivity shifts, $\Delta\theta$, was converted into mass surface coverage, Γ (ng/cm²), using the de Feijter equation:^{29,30} $\Gamma = \Delta\theta kd / (dn/dc)$, where dn/dc is the refractive index increment of a dense layer of GOx (1.77×10^{-10} cm³/ng),³¹ and kd is a SPR substrate-dependent

parameter provided by BioNavis with a value of 1.9×10^{-7} cm/deg. For ErGO and pErGO measurements, electrochemical reduction was performed in situ connecting a three-electrode electrochemical cell to the SPR instrument, where the SPR gold substrate was used as working electrode, a platinum wire as counter electrode and an Ag/AgCl wire as pseudo-reference electrode.

Construction of Glucose Oxidase-Functionalized Electrodes. GO-, pErGO-, and ErGO-coated substrates were modified with GOx by simply contacting them with a 10 μ M GOx solution in PBS buffer for 1 h. Afterward, electrodes were rinsed abundantly with PBS buffer to remove any unbound enzyme.

Electrochemical Measurements. CV and EIS experiments were performed with an Autolab PGSTAT302N potentiostat (Metrohm) in a conventional three-electrode Teflon electrochemical cell with a 0.18 cm² window equipped with an Ag/AgCl (3 M KCl) reference electrode and a platinum mesh counter electrode. Measurements were carried out at 22 °C. All electrode potentials cited in this work were measured against Ag/AgCl (3 M KCl). CV measurements were taken at a scan rate of 10 mV/s from -0.2 to 0.7 V in PBS buffer containing 1 mM ferrocenemethanol as redox mediator. Electrocatalysis measurements were performed at 10 mV/s at different glucose concentrations. Impedance spectra in the range 10^6 – 10^{-1} Hz were recorded with 10 mV rms AC perturbation at 0.25 V in PBS buffer containing 1 mM ferrocenemethanol. A Randles equivalent circuit, $R_s(CPE-[R_{CT}W])$, could be satisfactorily fitted to all EIS data. R_s accounts for the solution resistance, R_{CT} , the charge-transfer resistance, CPE, the constant phase element, which models the double layer capacitance, and W , the Warburg impedance, resulting from the diffusion of the electroactive probe from the electrolyte to the electrode surface.

RESULTS AND DISCUSSION

LB Assembly of GO Thin Films. Flat GO single layers were transferred to an ITO-glass substrate with accurate control over the film density and thickness by means of LB technique. The as-prepared GO colloidal dispersion was spread on the water–air interface of the LB trough drop-by-drop using a glass syringe. Since the LB interface is very sensitive to surface impurities, all the LB trough parts were carefully cleaned prior use. Before isothermal compression, the GO monolayer formed was stabilized for 15 min, obtaining invariable values for surface pressure. The surface pressure was monitored during the monolayer compression. Figure 1 shows the isothermal compression curve (surface pressure vs subphase area) corresponding to the phase transition of GO sheets. GO monolayers were transferred on ITO-coated glass at 15 mN/m at a pulling speed of 0.1 mm/min. The films obtained at these conditions exhibited interconnected GO flakes without major wrinkles or overlapping as can be observed from the SEM and AFM images of the LB-assembled GO flakes. AFM analysis for the different GO-based films showed similar roughness profiles (Figure S1). At higher surface pressure, the GO flakes tended to wrinkle compromising the exposure of functional groups that might potentially bind to a biomolecule, while at lower surface pressure the obtained GO assemblies consisted of isolated GO flakes. The wrinkle formation can be attributed to the presence of hydrogen bonds between carboxylic acid edges which favors the interactions between GO edges preventing them from

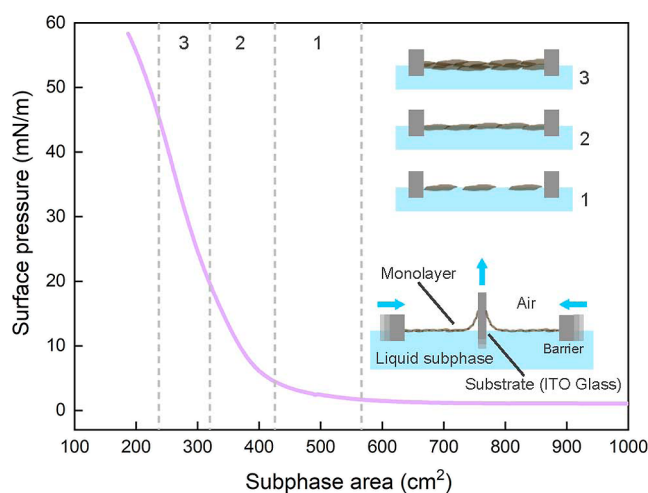


Figure 1. Surface pressure vs subphase area plot corresponding to the formation of the LB assembly of GO onto ITO-coated glass. Dashed lines correspond to different compression stages of GO monolayer.

sliding.²⁴ Lower pulling speeds on the other side favored obtaining flat GO flakes by allowing water evaporation during the transfer process.^{32,33}

Electrochemical Reduction of LB GO Thin Films. The chemical reduction of GO in solution is considered as the fastest way to produce rGO. Typically, a strong reducing agent as hydrazine monohydrate, hydroxylamine, phenylenediamine, sodium borohydride, and hydroquinone is used.¹⁰ However, the reduction of the oxygen-containing functional groups on the GO sheets affects their chemical interactions resulting in a less stable monolayer on water–air interface.³⁴ This poses a limitation to the preparation of rGO LB thin films. Conversely, thermal reduction is particularly appealing to prepare rGO sheets with controlled structural and electrical properties.³⁵ On the downside, this method requires long processing time and special precautions need to be taken to avoid the destruction of the basal plane during the reduction process. Alternatively, rGO thin films with similar chemical composition to that obtained by thermal annealing can be made by electrochemical reduction in a matter of minutes (Figure S2).

GO LB thin films supported on ITO-coated glass substrates were electrochemically reduced by performing cyclic voltammetry in PBS buffer solution (pH 7.4) with a potential window from 0.0 to -1.1 V (vs Ag/AgCl). The lower potential limit was set at -1.1 V to prevent the electrochemical reduction of ITO.¹⁵ Figure 2 shows repetitive cyclic voltammograms (ten cycles) for a GO/ITO electrode in PBS buffer solution. It can be observed during the first cathodic scan a small shoulder at -0.4 V and an intense, well-defined peak at -1.0 V, whereas no anodic peaks were noticed in the reverse scan. The first signal can be attributed to the reduction of residual molecular oxygen to hydrogen peroxide,³⁶ while the second reduction feature can be assigned mainly to the reduction of carbonyl and epoxy groups.^{37,38} In the consecutive cycles, a noticeable reduction in cathodic current can be observed, indicating that a significant portion of the oxygen functional groups was reduced during the first cycle. Thus, rGO sheets with different relative content of oxygen-containing groups were prepared by subjecting the electrodes to different reduction cycles. Partially electrochemically reduced GO (pErGO) and fully electrochemically reduced GO (ErGO) were obtained after 1 and 10 cycles, respectively.

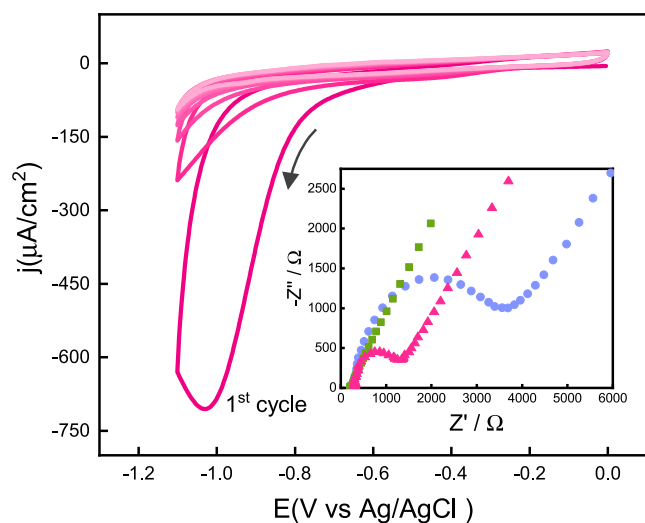


Figure 2. Cyclic voltammograms corresponding to the electrochemical reduction of GO/ITO in PBS pH 7.4 at 50 mV/s. The black line arrow indicates the direction of the potential scan. The inset shows the Nyquist plots for GO/ITO (blue circles), pErGO/ITO (magenta triangles), and ErGO/ITO (green squares) in PBS containing 1 mM ferrocenemethanol.

The inset in Figure 2 shows the Nyquist plots for the different electrodes in PBS buffer containing 1 mM ferrocenemethanol. Data could be fitted by a Randles equivalent circuit, $R_s(CPE[R_{CT}W])$, where R_s is the solution resistance, CPE accounts for the double layer capacitance, R_{CT} is the Faradaic charge-transfer resistance, and W is the Warburg impedance, which results from the impedance of the current due to diffusion from bulk solution to the interface. It can be observed that the semicircle diameter becomes smaller with increasing number of reduction cycles, which indicates a lower charge-transfer resistance (R_{CT}) between the redox mediator and the electrode surface. The R_{CT} of GO/ITO was 2.70 k Ω , while this value decreased to 1.15 and 0.09 k Ω for pErGO and ErGO, respectively. This can be attributed to the improved electro-transfer properties provided by the removal of the oxygen-containing functional groups.

XPS Characterization of GO Films. The electrochemically reduced GO/ITO electrodes were further characterized by XPS, as shown in Figure 3 for the C 1s photoionization region. GO supported on ITO prior to any electrochemical treatment exhibited two broad peaks at a binding energy range of 281–291 eV. Deconvolution of this signal showed the presence of six contributions, as in Table 1 shows. The intense peak with binding energy of 284.6 eV can be assigned to graphitic carbon (sp^2 -bonded C), while the component peak at 285.3 eV can be attributed to sp^3 -bonded C. Together, these signals account for 47.7% of the total C 1s intensity. Peaks at 286.3, 287.0, 288.1, and 289.2 eV are assigned to C–OH (hydroxyl), C–O–C (epoxy), C=O (carbonyl), and C(=O)OH (carboxyl) groups, respectively.^{25–28} From the percentages listed in Table 1, it can be seen that the carbonyl groups are the dominant surface oxygen-containing functional group on GO.

The effect of the electrochemical reduction on the surface oxygen content of the electrodes can be observed in the C 1s XPS spectra of pErGO and ErGO. In both samples, the most evident change is the decrease of the C=O-associated peak at 288.1 eV. In the case of pErGO, the relative intensity of the

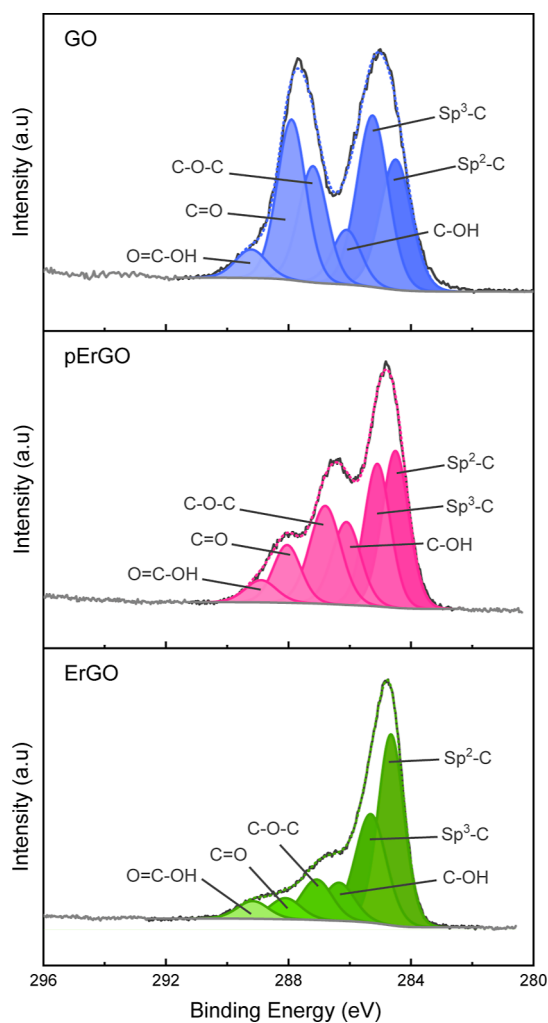


Figure 3. C 1s XPS spectra of a GO-based electrodes before electrochemical treatment (GO) and after electrochemical reduction performed by cyclic voltammetry at 50 mV/s in PBS pH 7.4 for one (pErGO) and ten cycles (ErGO), respectively.

Table 1. Binding Energy and Percent Atomic Ratios (%)^a Fitted from C 1s XPS Spectra

| signal peak | binding Energy (eV) | GO | sample pErGO | ErGO |
|-------------|---------------------|------|--------------|------|
| sp^2 -C | 284.6 | 20.6 | 26.7 | 41.2 |
| sp^3 -C | 285.3 | 27.1 | 23.9 | 28.2 |
| C–OH | 286.3 | 7.9 | 15.2 | 9.9 |
| C–O–C | 287.0 | 16.8 | 19.6 | 10.5 |
| C=O | 288.1 | 23.2 | 10.2 | 5.5 |
| O=C–OH | 289.2 | 4.5 | 4.4 | 4.6 |

^aValues are calculated relative to the signal of the total amount of C.

C=O signal reduced from 23.2 to 10.2%, while for ErGO, the contribution from carbonyl groups to the total amount of C was further reduced to 5.5%. This change was accompanied by an increase in the relative intensity of the C–OH signal (15.2 and 9.9% for pErGO and ErGO, respectively) as a consequence of the reduction of C–O–C and C=O moieties.³⁹ The relative intensity of the C(=O)OH signal, on the other side, remained nearly invariable between conditions confirming that the reduction potential limit was not negative enough to promote the reduction of the carboxyl groups.⁴⁰ The intensity of the peak assigned to the sp^2 C=C

bonding increased with the reduction process, which is consistent with the partial restoration of the sp^2 carbon network of graphene.¹⁴ Meanwhile, the contribution of the sp^3 carbon to the total C envelope showed no significant differences.

The results obtained from the XPS data confirm that electrochemical reduction of LB GO films supported on ITO, as conducted here, was effective to prepare rGO-based electrodes with different degrees of oxidation. Partial reduction of GO provided substrates with reactive surface oxygen groups as binding sites, while partially maintaining the electrical performance of graphene as expected from the level of sp^2 structure restoration.

Assembly of GOx onto LB GO Thin Films. GO/ITO electrodes subjected to electrochemical reduction, as described in the previous section, were treated with a solution of GOx in PBS buffer to build-up the chemoresponsive biointerfaces. Epoxy and carbonyl groups on the surface of GO can be used for the conjugation of GOx in a simple one-step procedure. Terminal primary amine groups in lysine residues of GOx react with epoxy and carbonyl groups to form secondary amines and Schiff bases, respectively.⁴¹ Therefore, tuning the content of oxygen surface functional groups allows for controlling GOx loading and consequently the responsiveness of the GOx-containing assembly.

To assess the capacity for functionalization of the GO-based electrodes, SPR experiments were conducted under saturation conditions, i.e., 10 μ M GOx. GO was first deposited on gold-coated glass slides by LB deposition following the same procedure as described for the preparation of GO/ITO substrates. Electrochemical reduction of GO to produce pErGO and ErGO was carried out using an electrochemical flow cell integrated within the SPR setup. Figure 4 depicts

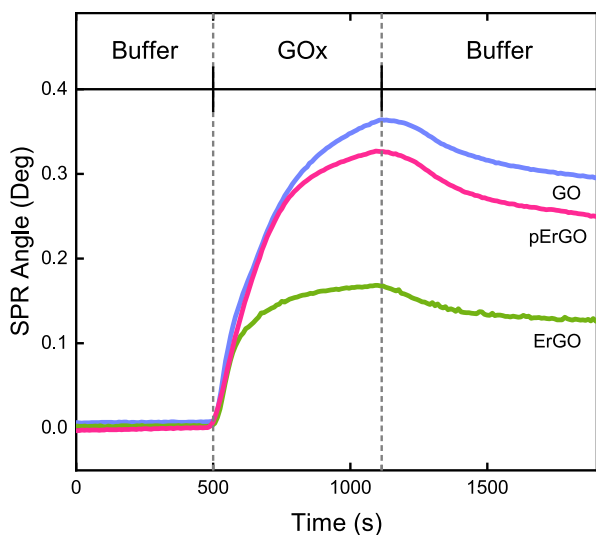


Figure 4. Time-resolved SPR sensorgrams for the adsorption of GOx in PBS buffer onto GO (blue), pErGO (magenta), and ErGO (green).

changes in the angle of minimum reflectance (θ_{\min}) when GOx interacts with the GO-based gold-coated sensors. SPR signal originates from changes in the refractive index as buffer solution is displaced by the adsorbed molecule. The initial exposure to the GOx solution led to a rapid increase in θ_{\min} followed by a plateau for all the substrates. Rinsing with PBS

buffer to remove unbound GOx did not evidence major changes in θ_{\min} demonstrating that the enzyme was efficiently bound to the substrate.

It can be observed that the GOx loading capacity of the substrates increases with the oxidation degree of GO, which is consistent with the surface concentration of epoxy and carbonyl groups obtained by XPS. The SPR angular shifts were converted into mass uptake using the de Feijter equation (Table S2).^{29,30} The SPR signal change corresponding to the adsorption of GOx on GO was 0.30° , which translates into 1.05×10^{-12} mol/cm², while protein coverage on pErGO and ErGO was 0.92×10^{-12} mol/cm² and 0.46×10^{-12} mol/cm², respectively. Furthermore, the ratio between the mass uptake of GOx and the combined relative concentration of C–O–C and C=O obtained by XPS was similar for all the studied conditions (Table S2). Similar results were obtained when GO-based surfaces were functionalized with aminoferrocene using the same procedure as that used for GOx. N 1s and C 1s XPS spectra analysis confirmed that large amounts of C–NH–C and C=N–C were formed, consistent with Schiff bases and secondary amines as result of the reaction between carbonyl and epoxy groups with amino groups, respectively (Figure S3, Tables S3 and S4). These results confirm that, under the experimental conditions employed, the immobilization of GOx proceeds mainly through covalent bonding, rather than by π -stacking interactions as reported for other proteins.⁴² Non-covalent π - π stacking occurs between the rings of graphene or its derivatives, and aromatic amino acids on the surface of the protein.⁴³ In the case of GOx, these hydrophobic interactions might be hampered because of the highly glycosylated nature of the enzyme.⁴⁴

Electrocatalytic Behavior of GOx-Functionalized GO-Based Electrodes. The cyclic voltammograms in Figure 5 exhibited well-defined oxidation and reduction peaks of ferrocenemethanol for all the studied GOx assemblies in the absence of glucose (black trace). However, a closer inspection at the electrochemical response reveals that the more oxidized the graphene is, peak currents decreased, while peak-to-peak separation increased (Table S5). This behavior is consistent with an increment in the number of defects into the GO sheets, which in turn results in an increased work function and decreased electrical conductivity,^{45,46} in agreement with our previous EIS measurements (Figure 2). Increasing the oxidation level of graphene has a deleterious effect on its electron transfer activity, but on the other side, it leads to higher enzyme loadings, as was revealed by SPR (Figure 4). To assess how these features impact on the chemoresponsive activity of the bioassemblies, we measured the enzymatic activity of GOx toward glucose oxidation by cyclic voltammetry in the presence of ferrocenemethanol as redox mediator (Figure 5).⁴⁷

During the oxidation of glucose, the flavin prosthetic group of GOx, FAD, is reduced to FADH₂ by accepting electrons from glucose. FADH₂ is then oxidized back to FAD by reacting with the oxidized form of ferrocenemethanol.⁴⁸ The working electrode potential is swept linearly in the anodic direction to regenerate the oxidized form of the redox mediator, which triggers the enzymatic process to continue in a cycle. Typical catalytic waves in the presence of increasing concentration of glucose are evidenced for the different GOx-functionalized GO electrodes under different oxidation conditions (Figure 5). Interestingly, the electrochemical response reached its highest

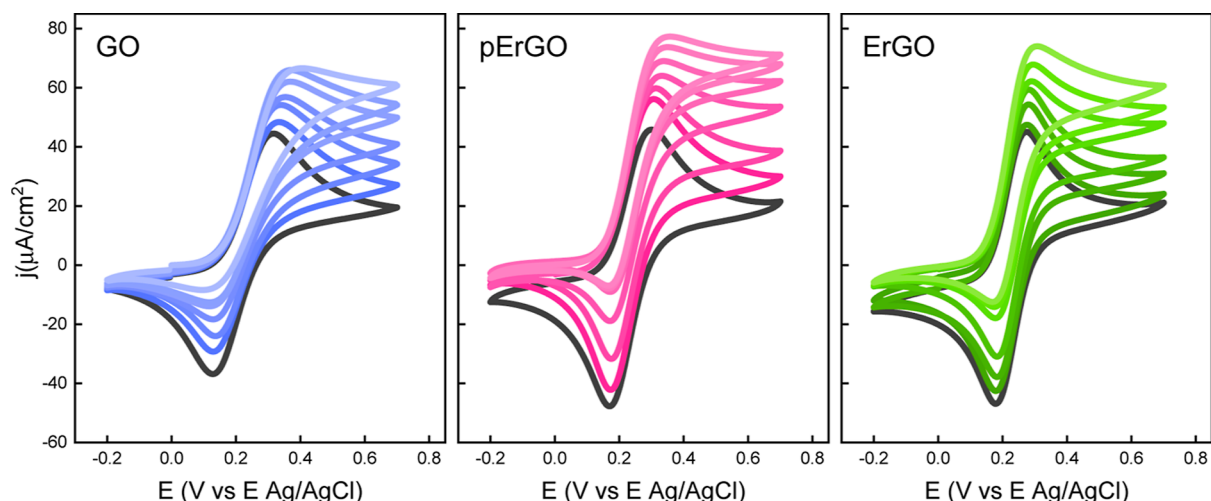


Figure 5. Voltammetric response of GOx assemblies in the presence of increasing amounts of glucose (0–10 mM), with 1 mM ferrocenemethanol as redox mediator, in PBS pH 7.4 at 22 °C. Scan rate: 10 mV/s.

value for GOx/pErGO electrodes where both enzyme density and electrical conductivity have intermediate levels.

In Figure 6, the bioelectrocatalytic current, j_{cat} is plotted as a function of the concentration of glucose for the different GOx/

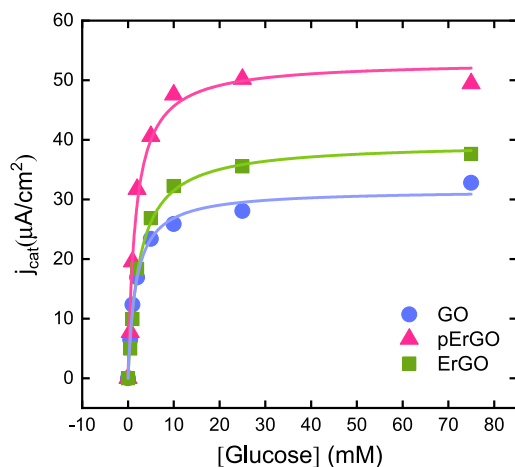


Figure 6. Catalytic response of GOx-coated GO-based electrodes as a function of the concentration of glucose with 1 mM ferrocenemethanol as redox mediator, in PBS pH 7.4 at 22 °C. Scan rate: 10 mV/s.

GO electrodes. The value of j_{cat} is obtained from the experimental data presented in Figure 5 by subtracting the voltammetric curve in the absence of glucose. All conditions showed a typical Michaelis–Menten⁴⁹ behavior where the initial rise in catalytic current is linear (0–3 mM glucose). At high substrate concentration, the reaction rate reaches a plateau as the enzyme active site is saturated with substrate, as reported for similar systems.^{50–52} The apparent Michaelis–Menten constants (K_m) were estimated for the different GOx assemblies and presented in Table 2. It is observed that the electrodes containing pErGO yielded the higher sensitivity followed by ErGO and GO, respectively. Values in the same order of magnitude were measured for the enzyme free in solution (Figure S6, Table S6), suggesting that the adsorbed GOx on the GO-based interface retains its catalytic activity to a great extent. Moreover, no structural changes were observed

Table 2. Michaelis–Menten Kinetics Parameters for the Different GOx Assemblies^a

| | GO | pErGO | ErGO |
|--|----------------|----------------|----------------|
| K_m (mM) | 1.7 ± 0.1 | 1.7 ± 0.3 | 2.6 ± 0.2 |
| $J_{\text{cat,max}}$ ($\mu\text{A}/\text{cm}^2$) | 35.9 ± 0.5 | 53.2 ± 2.0 | 39.5 ± 0.8 |

^aParameters obtained from nonlinear regression fitting to the Michaelis–Menten equation using the data presented in Figure 6.

that might compromise the integrity of the bioelectrodes (Figures S7 and S8). Interestingly, $J_{\text{cat,max}}$ takes its maximum value for pErGO, albeit the surface concentration of GOx is not the highest compared to the other conditions. The improvement of the bioelectrocatalytic response when pErGO is used as scaffold for the immobilization of GOx may be attributed to an enhanced electron transfer between ferrocenemethanol and the electrode surface. This is consistent with the results obtained for ErGO, where although the surface coverage of GOx is less than half of that of GO, the bioelectrocatalytic currents measured were higher. These findings highlight the relevance of tuning the surface chemistry of GO sheets in order to maximize the responsiveness of the biointerface.

The fabricated bioelectrodes exhibited a sensitivity that ranges from 8.3 to 16.1 $\mu\text{A mM}^{-1} \text{cm}^{-2}$ for GO with different degrees of oxidation with a linear range up to 3.5 mM for pErGO (Table 3). The pErGO electrodes exhibited a detection limit of 22.3 μM for glucose determination, whereas the GO and ErGO electrodes displayed higher values of 57.9 and 59.1 μM , respectively. The comparison of the responsive LB GO electrodes presented in this work with other GOx GO-based electrodes is shown in Table 3. Our approach yielded bioelectrodes with moderate sensitivity in comparison with other similar works,^{53–64} with the pErGO electrode showing the highest performance among our tested set. This can be attributed to the lower enzyme coverage obtained when GOx is linked to the surface of GO through direct covalent binding in contrast with approaches based on polymer-based composite materials.^{53,55,56,59,60,62,64} However, it is noteworthy to highlight that in terms of efficiency per enzyme unit, the enzymatic GO-based electrodes presented in this work demonstrate clear superiority. This indicates an effective harnessing of the catalytic potential of the enzyme, maximizing

Table 3. Comparison of the Performance of Different Graphene-Based GOx Electrodes

| modified electrode | sensitivity (<i>S</i>) ($\mu\text{A mM}^{-1}\text{cm}^{-2}$) | LOD ^a (μM) | linear range (mM) | S/Γ_{GOx}^b ($\mu\text{A}\cdot\text{ng}\cdot\text{mM}^{-1}$) | fabrication method | refs |
|---|---|---------------------------------------|----------------------|---|---------------------------|-----------|
| ErGO-MWCNT/Nf ^c | 7.95 | 4.7 | 0.01–6.5 | 1.39×10^{-4} | physisorption | 53 |
| rGO-AuNPs/GCE ^d | 0.083 | 10.0 | 1.0–8.0 | 1.47×10^{-6} | physisorption | 54 |
| rGO-HAp/GCE ^e | 16.9 | 30.0 | 0.1–11.5 | 6.54×10^{-5} | physisorption | 55 |
| GR/MnO ₂ /Nf ^f | 3.3 | 10.0 | 0.04–2 | 1.18×10^{-4} | physisorption | 56 |
| GN/FAD/apo-GOx ^g | ND | 110 | 1.4–11.0 | | mediated covalent binding | 57 |
| rGO-PtNPs-/GCE ^h | 27.5 | 1.2 | 2–10 | 6.3×10^{-3} | mediated covalent binding | 58 |
| ErGO-PLL/GCE ⁱ | 8.00 | 2.0 | 1.0–9.0 | 3.04×10^{-3} | physisorption | 59 |
| AuNPs/PANI/rGO/NH ₂ -MWCNTs ^j | 246.0 | 63.0 | 1–10 | | physisorption | 60 |
| DGNs/GRE ^k | ND | 22.0 | 0.1–10 | | mediated covalent binding | 61 |
| CNT/PEI ^l | 63.4 | 70 | 0.07–0.7 | | physisorption | 62 |
| GO-AuNP/GFE ^m | ND | 1.2 | ND | | physisorption | 63 |
| GA/cGO-CS/Au@Pd ⁿ | 64.2 | 10.4 | 0.02–4.2 | | cross-linked | 64 |
| pErGO/ITO | 16.1 | 22.3 | 0.1–3.5 | 0.11 | direct covalent binding | this work |
| GO/ITO | 8.3 | 57.9 | 0.1–3.0 | 0.05 | direct covalent binding | this work |
| ErGO/ITO | 9.1 | 59.1 | 0.1–3.5 | 0.12 | direct covalent binding | this work |

^aLOD is calculated as $3S_b/S$, where S_b is the standard deviation of the blank signal and S is the sensitivity. ^b S/Γ_{GOx} is the sensitivity normalized by the GOx surface coverage (Γ). ^cMWCNT multiwalled carbon nanotubes; Nf nafion. ^dAuNP_s gold nanoparticles; GCE glassy carbon electrode. ^eHAp hidroxiapatite. ^fGR graphene; MnO₂ manganese dioxide. ^gGN graphene nanoribbons; FAD flavin adenine dinucleotide; apo-GOx apoenzyme glucose oxidase. ^hPtNPs platinum nanoparticles. ⁱPLL poly-(L-lysine). ^jPANI polyaniline; NH₂-MWCNTs amine terminated multiwalled carbon nanotubes. ^kDGNs dendritic gold nanostructures; GRE graphitic rod electrode. ^lCNT carbon nanotubes; PEI polyethyleneimine. ^mGFE graphite fiber electrode. ⁿGA glutaraldehyde; cGO carboxylated GO; CS chitosan; Au@Pd gold-palladium core shell nanoparticles.

its utilization. These characteristics indicate that the attachment of GOx onto GO as described here allows unrestricted access to its active site without impairing its catalytic activity.

The interaction of graphene derivatives and enzymes has been previously investigated. During the adsorption process, enzymes undergo structural and functional changes. Wei and Ge reported that GO inhibited the activity of catalase by inducing the loss of α -helix and unfolding of the protein skeleton.⁶⁵ Similar effects were observed by other groups for different proteins.^{66–69} This is also the case for GOx.^{70–72} Liang et al. reported that upon GOx adsorption on GO a massive structural rearrangement takes place, which is responsible for shortening the distance of FAD to the surface of GO.⁷¹ As a result, direct electron transfer of GOx is facilitated but enzyme activity is lost. However, this effect is attenuated by reducing the density of oxygen-containing groups on GO. Even so, in terms of the electrode activity toward glucose oxidation, it is crucial to adjust the surface chemistry of GO that favor enzyme loading without compromising enzyme activity and electron transfer functionality.

CONCLUSIONS

In this study, we developed functional bioelectronic platforms by adsorbing GOx on GO/ITO electrodes. Our aim was to optimize the surface chemistry of GO for improved performance in biosensing applications. The presence of oxygen functional groups on GO enabled direct immobilization of GOx onto the electrodes by contacting them with the enzyme solution. By controlling the surface chemistry of GO, we could modulate the enzyme loading and overall chemoresponsiveness of the enzymatic electrodes. The immobilization of GOx on GO-based films was primarily governed by the reaction between the primary amine groups in lysine residues of GOx

and the epoxy and carbonyl groups on the GO surface. As expected, reducing the oxygen content of GO (ErGO) resulted in decreased GOx loading capacity while increasing the electrical conductivity of the films. This emphasized the importance of chemically adjusting the oxidation state of GO to enhance the efficiency of the electrochemical transducer. Through systematic analysis, we found that optimal responsiveness of the enzymatic films could be achieved by adjusting the oxygen content of GO to intermediate values (pErGO). We demonstrated that under the immobilization conditions used, the catalytic activity of GOx toward glucose oxidation was comparable to that observed in solution. The use of Langmuir–Blodgett assembly to prepare GO-based electrodes with electrochemically tuned surface chemistry proved to be a versatile strategy for creating highly functional interfaces. The presence of oxygen functional groups on the GO surface made it attractive for direct enzyme immobilization. Comparing with other sensors, enzymatic GO-based electrodes in this study show superior efficiency per enzyme unit, effectively utilizing the catalytic potential of the enzyme without compromising its activity. This approach can be extended to other biomolecules and substrates with large surface areas, enabling the development of various biosensing platforms beyond electrochemical readout. For example, we showed that SPR sensors coated with GO exhibited high sensitivity to interfacial molecular binding, which could be further enhanced by tuning the oxygen content of GO.

ASSOCIATED CONTENT

Supporting Information


The Supporting Information is available free of charge at <https://pubs.acs.org/doi/10.1021/acsomega.3c03220>.

Additional experimental details, characterization of materials, and electrocatalytic activity of GOx in solution (PDF)

AUTHOR INFORMATION

Corresponding Authors


Félix G. Requejo – Instituto de Investigaciones Fisicoquímicas Teóricas y Aplicadas (INIFTA), Universidad Nacional de La Plata, CONICET, La Plata 1900, Argentina;
Email: requejo@inifta.unlp.edu.ar

Diego Pallarola – Instituto de Nanosistemas, Universidad Nacional de General San Martín, San Martín 1650, Argentina;  orcid.org/0000-0001-5063-4288;
Email: dpallarola@unsam.edu.ar

Authors

Juan M. Devida – Instituto de Investigaciones Fisicoquímicas Teóricas y Aplicadas (INIFTA), Universidad Nacional de La Plata, CONICET, La Plata 1900, Argentina

Facundo Herrera – Instituto de Investigaciones Fisicoquímicas Teóricas y Aplicadas (INIFTA), Universidad Nacional de La Plata, CONICET, La Plata 1900, Argentina

M. Antonieta Daza Millone – Instituto de Investigaciones Fisicoquímicas Teóricas y Aplicadas (INIFTA), Universidad Nacional de La Plata, CONICET, La Plata 1900, Argentina;  orcid.org/0000-0002-4227-5868

Complete contact information is available at:

<https://pubs.acs.org/10.1021/acsomega.3c03220>

Notes

The authors declare no competing financial interest.

ACKNOWLEDGMENTS

This work was financially supported by the National Agency for the Promotion of Science and Technology (ANPCyT, PICT-2017-3944, PICT-2019-00905). This work has received funding from the European Union's Horizon 2020 research and innovation programme under the Marie Skłodowska-Curie grant agreement No 872869. D.P. acknowledges financial support from Max-Planck-Gesellschaft (Max Planck Partner Group Nanoelectronics for Cellular Interfaces INS/MPI-MR). F.G.R. acknowledges financial support from project X790, UNLP and PIP AÑO-0267 (CONICET). J.M.D. acknowledges CONICET for a doctoral scholarship. F.H. acknowledges CONICET for a postdoctoral fellowship. M.A.D.M., F.G.R., and D.P. are staff researchers of CONICET. We highly appreciate the support of Dr. Eduardo Prieto (INIFTA) and Dr. Jorge Donadelli (Y-TEC S.A.) during the AFM and XPS measurements, respectively.

REFERENCES

- (1) Krishnan, S. K.; Singh, E.; Singh, P.; Meyyappan, M.; Nalwa, H. S. A Review on Graphene-Based Nanocomposites for Electrochemical and Fluorescent Biosensors. *RSC Adv.* **2019**, *9*, 8778–8881.
- (2) Singh, E.; Meyyappan, M.; Nalwa, H. S. Flexible Graphene-Based Wearable Gas and Chemical Sensors. *ACS Appl. Mater. Interfaces* **2017**, *9*, 34544–34586.
- (3) Castro Neto, A. H.; Guinea, F.; Peres, N. M. R.; Novoselov, K. S.; Geim, A. K. The Electronic Properties of Graphene. *Rev. Mod. Phys.* **2009**, *81*, 109–162.
- (4) Kuc, A.; Heine, T.; Seifert, G. Structural and Electronic Properties of Graphene Nanoflakes. *Phys. Rev. B* **2010**, *81*, 085430.
- (5) Wang, G.; Jiang, N.; Xu, Y.; Zhang, Z.; Wang, G.; Cheng, K. Solvent-Assisted Assembly of Reduced Graphene Oxide/MXene-Polypyrrole Composite Film for Flexible Supercapacitors. *J. Colloid Interface Sci.* **2023**, *630*, 817–827.
- (6) Li, Z.; Chao, X.; Balilonda, A.; Chen, W. Scalable van Der Waals Graphene Films for Electro-Optical Regulation and Thermal Camouflage. *InfoMat* **2023**, *5*, No. e12418.
- (7) Lee, J.; Kim, J.; Kim, S.; Min, D.-H. Biosensors Based on Graphene Oxide and Its Biomedical Application. *Adv. Drug Delivery Rev.* **2016**, *105*, 275–287.
- (8) Wang, Q.; Jing, J.-Y.; Wang, B.-T. Highly Sensitive SPR Biosensor Based on Graphene Oxide and Staphylococcal Protein A Co-Modified TFBG for Human IgG Detection. *IEEE Trans. Instrum. Meas.* **2019**, *68*, 3350–3357.
- (9) Aliyev, E.; Filiz, V.; Khan, M. M.; Lee, Y. J.; Abetz, C.; Abetz, V. Structural Characterization of Graphene Oxide: Surface Functional Groups and Fractionated Oxidative Debris. *Nanomaterials* **2019**, *9*, 1180.
- (10) Agarwal, V.; Zetterlund, P. B. Strategies for Reduction of Graphene Oxide – A Comprehensive Review. *Chem. Eng. J.* **2021**, *405*, 127018.
- (11) Gómez-Navarro, C.; Meyer, J. C.; Sundaram, R. S.; Chuvilin, A.; Kurasch, S.; Burghard, M.; Kern, K.; Kaiser, U. Atomic Structure of Reduced Graphene Oxide. *Nano Lett.* **2010**, *10*, 1144–1148.
- (12) Erickson, K.; Erni, R.; Lee, Z.; Alem, N.; Gannett, W.; Zettl, A. Determination of the Local Chemical Structure of Graphene Oxide and Reduced Graphene Oxide. *Adv. Mater.* **2010**, *22*, 4467–4472.
- (13) Negishi, R.; Kobayashi, Y. Extraordinary Suppression of Carrier Scattering in Large Area Graphene Oxide Films. *Appl. Phys. Lett.* **2014**, *105*, 253502.
- (14) Shao, Y.; Wang, J.; Engelhard, M.; Wang, C.; Lin, Y. Facile and Controllable Electrochemical Reduction of Graphene Oxide and Its Applications. *J. Mater. Chem.* **2010**, *20*, 743–748.
- (15) Marrani, A. G.; Coico, A. C.; Giacco, D.; Zanon, R.; Motta, A.; Schrebler, R.; Dini, D.; Di Girolamo, D.; Dalchiele, E. A. Flexible Interfaces between Reduced Graphene Oxide and Indium Tin Oxide/Polyethylene Terephthalate for Advanced Optoelectronic Devices. *ACS Appl. Nano Mater.* **2019**, *2*, 5963–5972.
- (16) Guo, H.-L.; Wang, X.-F.; Qian, Q.-Y.; Wang, F.-B.; Xia, X.-H. A Green Approach to the Synthesis of Graphene Nanosheets. *ACS Nano* **2009**, *3*, 2653–2659.
- (17) Zhou, M.; Wang, Y.; Zhai, Y.; Zhai, J.; Ren, W.; Wang, F.; Dong, S. Controlled Synthesis of Large-Area and Patterned Electrochemically Reduced Graphene Oxide Films. *Chem. - Eur. J.* **2009**, *15*, 6116–6120.
- (18) Schniepp, H. C.; Li, J.-L.; McAllister, M. J.; Sai, H.; Herrera-Alonso, M.; Adamson, D. H.; Prud'homme, R. K.; Car, R.; Saville, D. A.; Aksay, I. A. Functionalized Single Graphene Sheets Derived from Splitting Graphite Oxide. *J. Phys. Chem. B* **2006**, *110*, 8535–8539.
- (19) Gómez-Navarro, C.; Weitz, R. T.; Bittner, A. M.; Scolari, M.; Mews, A.; Burghard, M.; Kern, K. Electronic Transport Properties of Individual Chemically Reduced Graphene Oxide Sheets. *Nano Lett.* **2007**, *7*, 3499–3503.
- (20) Wang, X.; Zhi, L.; Müllen, K. Transparent, Conductive Graphene Electrodes for Dye-Sensitized Solar Cells. *Nano Lett.* **2008**, *8*, 323–327.
- (21) Chang, C. W.; Hon, M. H.; Leu, I. C. Patterns of Solution-Processed Graphene Oxide Produced by a Transfer Printing Method. *J. Electrochem. Soc.* **2012**, *159*, H605–H609.
- (22) Chen, L.; Tang, Y.; Wang, K.; Liu, C.; Luo, S. Direct Electrodeposition of Reduced Graphene Oxide on Glassy Carbon Electrode and Its Electrochemical Application. *Electrochem. Commun.* **2011**, *13*, 133–137.
- (23) Cote, L. J.; Kim, F.; Huang, J. Langmuir–Blodgett Assembly of Graphite Oxide Single Layers. *J. Am. Chem. Soc.* **2009**, *131*, 1043–1049.
- (24) Zheng, Q.; Ip, W. H.; Lin, X.; Yousefi, N.; Yeung, K. K.; Li, Z.; Kim, J.-K. Transparent Conductive Films Consisting of Ultralarge

Graphene Sheets Produced by Langmuir–Blodgett Assembly. *ACS Nano* **2011**, *5*, 6039–6051.

(25) Marcano, D. C.; Kosynkin, D. V.; Berlin, J. M.; Sinitskii, A.; Sun, Z.; Slesarev, A.; Alemany, L. B.; Lu, W.; Tour, J. M. Improved Synthesis of Graphene Oxide. *ACS Nano* **2010**, *4*, 4806–4814.

(26) Sutar, D. S.; Narayanam, P. K.; Singh, G.; Botcha, V. D.; Talwar, S. S.; Srinivasa, R. S.; Major, S. S. Spectroscopic Studies of Large Sheets of Graphene Oxide and Reduced Graphene Oxide Monolayers Prepared by Langmuir–Blodgett Technique. *Thin Solid Films* **2012**, *520*, 5991–5996.

(27) Priante, F.; Salim, M.; Ottaviano, L.; Perrozzi, F. XPS Study of Graphene Oxide Reduction Induced by (100) and (111)-Oriented Si Substrates. *Nanotechnology* **2018**, *29*, 075704.

(28) Al-Gaashani, R.; Najjar, A.; Zakaria, Y.; Mansour, S.; Atieh, M. A. XPS and Structural Studies of High Quality Graphene Oxide and Reduced Graphene Oxide Prepared by Different Chemical Oxidation Methods. *Ceram. Int.* **2019**, *45*, 14439–14448.

(29) De Feijter, J. A.; Benjamins, J.; Veer, F. A. Ellipsometry as a Tool to Study the Adsorption Behavior of Synthetic and Biopolymers at the Air–Water Interface. *Biopolymers* **1978**, *17*, 1759–1772.

(30) Knoll, W. Interfaces and Thin Films as Seen by Bound Electromagnetic Waves. *Annu. Rev. Phys. Chem.* **1998**, *49*, 569–638.

(31) Forzani, E. S.; Otero, M.; Pérez, M. A.; Teijelo, M. L.; Calvo, E. J. The Structure of Layer-by-Layer Self-Assembled Glucose Oxidase and Os(Bpy)₂ ClPYCH₂ NH–Poly(Allylamine) Multilayers: Ellipsometric and Quartz Crystal Microbalance Studies. *Langmuir* **2002**, *18*, 4020–4029.

(32) Kim, J.; Kim, F.; Huang, J. Seeing Graphene-Based Sheets. *Mater. Today* **2010**, *13*, 28–38.

(33) Zheng, Q.; Shi, L.; Ma, P.-C.; Xue, Q.; Li, J.; Tang, Z.; Yang, J. Structure Control of Ultra-Large Graphene Oxide Sheets by the Langmuir–Blodgett Method. *RSC Adv.* **2013**, *3*, 4680.

(34) Fadil, Y.; Dinh, L. N. M.; Yap, M. O. Y.; Kuchel, R. P.; Yao, Y.; Omura, T.; Aregueta-Robles, U. A.; Song, N.; Huang, S.; Jasinski, F.; Thickett, S. C.; Minami, H.; Agarwal, V.; Zetterlund, P. B. Ambient-Temperature Waterborne Polymer/RGO Nanocomposite Films: Effect of RGO Distribution on Electrical Conductivity. *ACS Appl. Mater. Interfaces* **2019**, *11*, 48450–48458.

(35) Yin, K.; Li, H.; Xia, Y.; Bi, H.; Sun, J.; Liu, Z.; Sun, L. Thermodynamic and Kinetic Analysis of Low-Temperature Thermal Reduction of Graphene Oxide. *Nano-Micro Lett.* **2011**, *3*, 51–55.

(36) Nissim, R.; Compton, R. G. Superoxide Generation from the Reduction of Oxygen at the Carbon–Oil–Water Triple Phase Boundary. *Phys. Chem. Chem. Phys.* **2013**, *15*, 11918.

(37) Kauppila, J.; Kunnas, P.; Damlin, P.; Viinikanoja, A.; Kvarnström, C. Electrochemical Reduction of Graphene Oxide Films in Aqueous and Organic Solutions. *Electrochim. Acta* **2013**, *89*, 84–89.

(38) Zhang, Y.; Hao, H.; Wang, L. Effect of Morphology and Defect Density on Electron Transfer of Electrochemically Reduced Graphene Oxide. *Appl. Surf. Sci.* **2016**, *390*, 385–392.

(39) Marrani, A. G.; Zanoni, R.; Schrebler, R.; Dalchiele, E. A. Toward Graphene/Silicon Interface via Controlled Electrochemical Reduction of Graphene Oxide. *J. Phys. Chem. C* **2017**, *121*, 5675–5683.

(40) Marrani, A. G.; Motta, A.; Schrebler, R.; Zanoni, R.; Dalchiele, E. A. Insights from Experiment and Theory into the Electrochemical Reduction Mechanism of Graphene Oxide. *Electrochim. Acta* **2019**, *304*, 231–238.

(41) Alwarappan, S.; Liu, C.; Kumar, A.; Li, C.-Z. Enzyme-Doped Graphene Nanosheets for Enhanced Glucose Biosensing. *J. Phys. Chem. C* **2010**, *114*, 12920–12924.

(42) Zhang, Y.; Zhang, J.; Huang, X.; Zhou, X.; Wu, H.; Guo, S. Assembly of Graphene Oxide–Enzyme Conjugates through Hydrophobic Interaction. *Small* **2012**, *8*, 154–159.

(43) Karimi, A.; Othman, A.; Uzunoglu, A.; Stanciu, L.; Andreescu, S. Graphene Based Enzymatic Bioelectrodes and Biofuel Cells. *Nanoscale* **2015**, *7*, 6909–6923.

(44) Kalisz, H. M. K.; Hecht, H.-J.; Schomburg, D.; Schmid, R. D. Effects of Carbohydrate Depletion on the Structure, Stability and Activity of Glucose Oxidase from *Aspergillus Niger*. *Biochim. Biophys. Acta* **1991**, *1080*, 138–142.

(45) Gao, M.; Xu, Y.; Wang, X.; Sang, Y.; Wang, S. Analysis of Electrochemical Reduction Process of Graphene Oxide and Its Electrochemical Behavior. *Electroanalysis* **2016**, *28*, 1377–1382.

(46) Rychagov, A. Yu.; Gubin, S. P.; Chuprov, P. N.; Kornilov, D. Yu.; Karaseva, A. S.; Krasnova, E. S.; Voronov, V. A.; Tkachev, S. V. Electrochemical Reduction and Electric Conductivity of Graphene Oxide Films. *Russ. J. Electrochem.* **2017**, *53*, 721–727.

(47) Pallarola, D.; Queralto, N.; Battaglini, F.; Azzaroni, O. Supramolecular Assembly of Glucose Oxidase on Concanavalin A–Modified Gold Electrodes. *Phys. Chem. Chem. Phys.* **2010**, *12*, 8071.

(48) Demaille, C.; Moiroux, J.; Savéant, J. M. Multilayers on Electrodes. *Protein Architecture: Interfacing Molecular Assemblies and Immobilization Biotechnology*; CRC Press, 1999; Vol. 75; p 311.

(49) Cornish-Bowden, A. Estimation of Kinetic Constants. In *Fundamentals of Enzyme Kinetics*; Elsevier, 1979; Chapter 10, pp 200–211.

(50) Pallarola, D.; Queralto, N.; Knoll, W.; Ceolin, M.; Azzaroni, O.; Battaglini, F. Redox-Active Concanavalin A: Synthesis, Characterization, and Recognition-Driven Assembly of Interfacial Architectures for Bioelectronic Applications. *Langmuir* **2010**, *26*, 13684–13696.

(51) Pallarola, D.; Queralto, N.; Knoll, W.; Azzaroni, O.; Battaglini, F. Facile Glycoenzyme Wiring to Electrode Supports by Redox-Active Biosupramolecular Glue. *Chem. - Eur. J.* **2010**, *16*, 13970–13975.

(52) Pallarola, D.; Bildering, C. v.; Pietrasanta, L. I.; Queralto, N.; Knoll, W.; Battaglini, F.; Azzaroni, O. Recognition-Driven Layer-by-Layer Construction of Multiprotein Assemblies on Surfaces: A Biomolecular Toolkit for Building up Chemoresponsive Bioelectrochemical Interfaces. *Phys. Chem. Chem. Phys.* **2012**, *14*, 11027.

(53) Mani, V.; Devadas, B.; Chen, S.-M. Direct Electrochemistry of Glucose Oxidase at Electrochemically Reduced Graphene Oxide–Multiwalled Carbon Nanotubes Hybrid Material Modified Electrode for Glucose Biosensor. *Biosens. Bioelectron.* **2013**, *41*, 309–315.

(54) Amouzadeh Tabrizi, M.; Varkani, J. N. Green Synthesis of Reduced Graphene Oxide Decorated with Gold Nanoparticles and Its Glucose Sensing Application. *Sens. Actuators, B* **2014**, *202*, 475–482.

(55) Bharath, G.; Madhu, R.; Chen, S.-M.; Veeramani, V.; Balamurugan, A.; Mangalaraj, D.; Viswanathan, C.; Ponpandian, N. Enzymatic Electrochemical Glucose Biosensors by Mesoporous 1D Hydroxyapatite-on-2D Reduced Graphene Oxide. *J. Mater. Chem. B* **2015**, *3*, 1360–1370.

(56) Liu, Y.; Zhang, X.; He, D.; Ma, F.; Fu, Q.; Hu, Y. An Amperometric Glucose Biosensor Based on a MnO₂/Graphene Composite Modified Electrode. *RSC Adv.* **2016**, *6*, 18654–18661.

(57) Mehmeti, E.; Stanković, D. M.; Chaiyo, S.; Zavanik, J.; Žagar, K.; Kalcher, K. Wiring of Glucose Oxidase with Graphene Nanoribbons: An Electrochemical Third Generation Glucose Biosensor. *Microchim. Acta* **2017**, *184*, 1127–1134.

(58) Akkaya, B.; Çakiroğlu, B.; Özacar, M. Tannic Acid-Reduced Graphene Oxide Deposited with Pt Nanoparticles for Switchable Bioelectronics and Biosensors Based on Direct Electrochemistry. *ACS Sustainable Chem. Eng.* **2018**, *6*, 3805–3814.

(59) Zhang, D.; Chen, X.; Ma, W.; Yang, T.; Li, D.; Dai, B.; Zhang, Y. Direct Electrochemistry of Glucose Oxidase Based on One Step Electrodeposition of Reduced Graphene Oxide Incorporating Polymerized L-Lysine and Its Application in Glucose Sensing. *Mater. Sci. Eng., C* **2019**, *104*, 109880.

(60) Maity, D.; Minitha, C. R.; Rajendra Kumar, R. T. Glucose Oxidase Immobilized Amine Terminated Multiwall Carbon Nanotubes/Reduced Graphene Oxide/Polyaniline/Gold Nanoparticles Modified Screen-Printed Carbon Electrode for Highly Sensitive Amperometric Glucose Detection. *Mater. Sci. Eng., C* **2019**, *105*, 110075.

(61) Sakalauskiene, L.; Popov, A.; Kausaitė-Minkstimiene, A.; Ramanavicius, A.; Ramanaviciene, A. The Impact of Glucose Oxidase

Immobilization on Dendritic Gold Nanostructures on the Performance of Glucose Biosensors. *Biosensors* **2022**, *12*, 320.

(62) Lin, M.-H.; Gupta, S.; Chang, C.; Lee, C.-Y.; Tai, N.-H. Carbon Nanotubes/Polyethylenimine/Glucose Oxidase as a Non-Invasive Electrochemical Biosensor Performs High Sensitivity for Detecting Glucose in Saliva. *Microchem. J.* **2022**, *180*, 107547.

(63) Han, Z.; Zhang, X.; Yuan, H.; Li, Z.; Li, G.; Zhang, H.; Tan, Y. Graphene Oxide/Gold Nanoparticle/Graphite Fiber Microelectrodes for Directing Electron Transfer of Glucose Oxidase and Glucose Detection. *J. Power Sources* **2022**, *521*, 230956.

(64) Güler, M.; Zengin, A.; Alay, M. Fabrication of Glucose Bioelectrochemical Sensor Based on Au@Pd Core-Shell Supported by Carboxylated Graphene Oxide. *Anal. Biochem.* **2023**, *667*, 115091.

(65) Wei, X.-L.; Ge, Z.-Q. Effect of Graphene Oxide on Conformation and Activity of Catalase. *Carbon* **2013**, *60*, 401–409.

(66) Bai, Y.; Ming, Z.; Cao, Y.; Feng, S.; Yang, H.; Chen, L.; Yang, S.-T. Influence of Graphene Oxide and Reduced Graphene Oxide on the Activity and Conformation of Lysozyme. *Colloids Surf., B* **2017**, *154*, 96–103.

(67) Feng, R.; Yu, Y.; Shen, C.; Jiao, Y.; Zhou, C. Impact of Graphene Oxide on the Structure and Function of Important Multiple Blood Components by a Dose-Dependent Pattern: Impact of GO on Structure and Function of Multiple Blood Components. *J. Biomed. Mater. Res.* **2015**, *103*, 2006–2014.

(68) Wang, Y.; Zhu, Z.; Zhang, H.; Chen, J.; Tang, B.; Cao, J. Investigation on the Conformational Structure of Hemoglobin on Graphene Oxide. *Mater. Chem. Phys.* **2016**, *182*, 272–279.

(69) Hernández-Cancel, G.; Suazo-Dávila, D.; Ojeda-Cruzado, A. J.; García-Torres, D.; Cabrera, C. R.; Griebenow, K. Graphene Oxide as a Protein Matrix: Influence on Protein Biophysical Properties. *J. Nanobiotechnol.* **2015**, *13*, 70.

(70) Zhou, L.; Jiang, Y.; Gao, J.; Zhao, X.; Ma, L.; Zhou, Q. Oriented Immobilization of Glucose Oxidase on Graphene Oxide. *Biochem. Eng. J.* **2012**, *69*, 28–31.

(71) Liang, B.; Guo, X.; Fang, L.; Hu, Y.; Yang, G.; Zhu, Q.; Wei, J.; Ye, X. Study of Direct Electron Transfer and Enzyme Activity of Glucose Oxidase on Graphene Surface. *Electrochem. Commun.* **2015**, *50*, 1–5.

(72) Zhou, L.; Jiang, Y.; Ma, L.; He, Y.; Gao, J. Immobilization of Glucose Oxidase on Polydopamine-Functionalized Graphene Oxide. *Appl. Biochem. Biotechnol.* **2015**, *175*, 1007–1017.